Journal of Sound and Vibration 332 (2013) 3654–3666

Contents lists available at SciVerse ScienceDirect

Journal of Sound and Vibration

journal homepage: www.elsevier.com/locate/jsvi

Bayesian characterization of Young's modulus of viscoelastic materials in laminated structures

E. Zhang [a,*], J.D. Chazot [a], J. Antoni [b], M. Hamdi [a]

[a] Roberval Laboratory of Mechanics, UMR 7337, University of Technology of Compiègne, 60205 Compiègne, France
[b] Laboratory Vibrations and Acoustics, University of Lyon, F-69621 Villeurbanne, France

ARTICLE INFO

Article history:
Received 3 April 2012
Received in revised form
12 December 2012
Accepted 26 February 2013
Handling Editor: K. Worden
Available online 26 March 2013

ABSTRACT

This paper addresses an inverse approach to estimate the frequency-dependent Young's modulus of a viscoelastic polymer layer in a laminated structure. The Young's modulus is parameterized by a fractional derivative model and examined from a Bayesian perspective with the consideration of measurement and modeling uncertainties. The probabilistic Bayesian identification is carried out based on an efficient surrogate model through the use of Markov Chain Monte Carlo sampling methods. The proposed approach is experimentally validated on laminated glass.

1. Introduction

Laminated structures are widely spread in contemporary industrial fields; for instance laminated glass is used for windshields in automotive industry. Laminated structures are typically formed by two plates bonded together with a polymeric adhesive. More than just a bond between two layers, the polymeric core can provide an interesting damping effect due to the high shear strains imposed by the external layers. Such polymer core of viscoelastic property is characterized by a temperature-frequency-dependent complex Young's modulus. In noise and vibration applications, the knowledge of this elastic modulus in a wide frequency band is required, e.g. for numerical simulation, damping design, and so on. The test technique and the related theory of viscoelastic damping materials have been thoroughly discussed in Ref. [1]. The basic idea to obtain the desired material properties consists in measuring the frequency and damping level of various bending resonances of a sample beam, then back-calculating the viscoelastic material properties from these modal data at discrete resonance frequencies. This is applied in the standard testing procedure [2] for the Young's modulus. Ref. [3] advocates the broadband modal analysis by system identification techniques to accurately estimate the resonances of a homogeneous viscoelastic beam and quantify their uncertainties due to the measurement noise and nonlinear distortions; from these estimated resonances, different kinds of beam models are used to obtain the Young's modulus.

Recently, more attention has been paid to the inverse estimation of the Young's modulus in a continuous broad frequency range, and not only just at resonant frequencies. The main idea of this approach is to estimate the Young's modulus parametrically by minimizing the residuals between indirect experimental data and predictions of a numerical model. The complex modulus of an adhesive layer is identified with a sandwich finite element (FE) model from experimental modal data [4]. The characterization of the Young's modulus is conducted for viscoelastic materials using a gradient-based optimization algorithm from frequency response functions (FRFs) based on a fractional derivative model [5] or a concept of internal variables [6]. Ref. [7] constructs the cost function from FRFs at user-controlled frequencies to make the method insensitive to the measurement noise, and applies the identification approach on high damping

* Corresponding author. Tel.: +32 (0)2 629 28 44.
E-mail addresses: erliang.zhang@vub.ac.be, npuzhangel@gmail.com (E. Zhang).

0022-460X/$ - see front matter © 2013 Elsevier Ltd. All rights reserved.
http://dx.doi.org/10.1016/j.jsv.2013.02.032

Nomenclature

d	modulus increment ratio
$F(k)$	input discrete spectrum
$H(\omega)$	frequency response function
$q(t)$	random phase multisine
$Y(k)$	output discrete spectrum
$\boldsymbol{\alpha}$	modal parameters
β	scale parameter of the Gamma distribution of $\boldsymbol{\gamma}$
$\mathcal{D}$	set of experimental data
$\boldsymbol{\gamma}$	weighting coefficients
τ	relaxation time
μ, ν	noninteger order derivatives
$\boldsymbol{\theta}$	modulus parameters
$\hat{X}$	sample mean of X
E_0	static Young's modulus
n_c	number of Markov chains
n_m	number of poles
n_s	sample number by Latin Hypercube sampling
n_{cluster}	number of clusters of $H(\omega)$
n_ω	number of frequency lines
$\mathbf{C}_{\text{exp}}$	covariance due to the measurement uncertainty
$\mathbf{C}_{\text{mod}}$	covariance due to the modeling uncertainty
$N_F(k)$,$N_Y(k)$	input–output noise spectra
$Y_S(k)$	nonlinear distortions
T_{ref}	reference temperature
β_0	scale parameter of the Gamma distribution of β
σ_X^2	variance of X

materials. Besides, the experiment development for the viscoelastic property identification is particularly considered in Ref. [8]. However, the measurement noise and the nonmodeled dynamics of the laminated structure are rarely taken into account explicitly for viscoelastic identification. As a matter of fact, measurements are corrupted by perturbations of various origins and numerical models are built based on assumptions and approximations. A probabilistic identification of the Young's modulus is therefore more adapted as it can deal properly with these uncertainties.

The goal of this paper is to identify the Young's modulus of the polymer core in a laminated structure by a probabilistic approach especially from a Bayesian perspective. The Bayesian method endows the parameters with prior information in the form of probability density function (pdf), which can be regarded as imposing soft physical constraints to force the problem to find a unique and stable solution; it also provides a rigorous probabilistic framework to account for most sources of errors that contribute to the uncertainty of the parameters to be inferred [9,10]. The Bayesian approach is proposed for structural dynamics in a pioneer work [11] and its related techniques are surveyed in [12]; and it has been also used to incorporate the modeling error for full-scale FE model updating [13]. The Bayesian probabilistic approach not only regards the Young's modulus as a random variable, but also considers the nonmodeled dynamics, called modeling uncertainty, aleatory due to the lack of knowledge by epistemic uncertainty.

In the present work, the Young's modulus is parameterized in a broad frequency band based on a fractional derivative model with a small set of parameters. Effort is particularly paid to the following ingredients in order to enable probabilistic modulus identification of a polymer core from FRF data of a layered structure. (1) A cost-effective surrogate model is constructed based on an artificial neural network (ANN) by means of data processing techniques to alleviate the Bayesian computation, (2) the measurement noise and nonlinear distortions, and the modeling uncertainty are taken into account explicitly in the formulation of the Bayesian modulus identification, and the latter is modeled in a hierarchical way and (3) the parameters of the modulus model and those characterizing the modeling uncertainty are jointly updated by exploring the posterior probability density function through the use of Markov Chain Monte Carlo (MCMC) methods. In addition to the above contributions, a laminated FE model with an accurate viscoelastic shell element is implemented to simulate structural responses, and a specific experimental protocol is adopted to estimate FRFs and quantify their uncertainties issued from the measurement noise and nonlinear distortions.

The paper is structured as follows. Section 2 presents the identification prerequisites which include the laminated FE formulation and the experiment protocol. Section 3 is devoted to constructing a complete and efficient Bayesian identification framework with the consideration of the measurement and modeling errors. Section 4 illustrates the methodology on experimental examples. Conclusions are drawn in Section 5.

2. Numerical model and measurements

The model reliability and measurement quality are fundamental for parameter estimation in an inverse way. So, in the following sections a FE model with a sophisticated laminated shell element and a specific experimental protocol for high quality measurements are introduced.

2.1. Laminated finite element model combined with Padé approximant

The complex elastic moduli of viscoelastic materials vary as a function of many parameters, most important of which are the temperature and the frequency. In fact, these two parameters are not independent. A frequency-temperature superposition principle exists and can be modeled for example with the WLF law [14]. This principle is frequently used in

dynamic mechanical analyzers to measure elastic moduli on a large frequency band. In the following the temperature effect is not taken into account. At a given reference temperature T_{ref}, the Young's modulus is described here by a fractional derivative model [15] with a small set of parameters

$$E(\omega,T_{\mathrm{ref}})=E_0\left[1+\frac{(d-1)(\mathrm{j}\omega\tau)^{\mu}}{1+(\mathrm{j}\omega\tau)^{\nu}}\right], \tag{1}$$

where E_0 is the modulus value at $\omega=0$, $d=E_\infty/E_0$ with E_∞ the modulus at $\omega\to\infty$, τ is the time of relaxation, $\mu,\nu\in[0,1]$ with $\mu\geq\nu$, and $\mathrm{j}^2=-1$. By virtue of this parametric modeling, the identification of the modulus in a broad frequency range is reduced to the estimation of these five parameters.

In general, the global behavior of laminated structures is more difficult to predict than homogeneous structures with isotropic material. The discontinuity of the mechanical properties at each layer interface can indeed lead to high shear strains in the internal layers. The displacements can also present singular points at these interfaces in some cases. The ZPST element presented in [16] is a multilayered shell finite element which works by approximating the through-the-thickness displacement using a p-order polynomial and a zig-zag function (see Fig. 1). It has been shown to be capable of modeling appropriately viscoelastic laminated structures in a previous work [17]. This ZPST element is therefore used in the present study. The governing equation of a laminated viscoelastic structure is

$$[\mathbf{K}(\omega,\boldsymbol{\theta})-\omega^2\mathbf{M}]\mathbf{U}(\omega)=\mathbf{F}(\omega), \tag{2}$$

where $\mathbf{F}(\omega)$ is the generalized nodal excitation, $\mathbf{U}(\omega)$ is the generalized nodal displacement with all the degrees of freedom, $\mathbf{K}(\omega,\boldsymbol{\theta})$ and $\mathbf{M}$ are the stiffness and mass matrices, respectively, and $\boldsymbol{\theta}$ is a vector concatenating the parameters of Eq. (1). Eq. (2) is solved at each frequency to obtain the nodal solution, which will be cumbersome to get the structural response of a large FE model at numerous frequencies. The Padé approximation is therefore implemented to accelerate the frequency sweep computation. Instead of solving Eq. (2) at each frequency on a fine grid, it is firstly solved on a user-chosen coarser grid (not necessarily regular). The response is then reconstructed on the fine grid by means of the Padé approximant. At a frequency, ω, on the user-chosen coarse grid, the nodal solution U_i at the ith degree of freedom (dof) is returned for the frequency $\omega+\delta\omega$ by the Padé approximant as

$$U_i(\omega+\delta\omega)=\frac{P(\delta\omega)}{Q(\delta\omega)}+\mathcal{O}[(\delta\omega)^{L+M+1}], \tag{3}$$

with the polynomials

$$P(\delta\omega)=\sum_{l=0}^{L}p_l\times(\delta\omega)^l,\ Q(\delta\omega)=1+\sum_{m=1}^{M}q_m\times(\delta\omega)^m. \tag{4}$$

The Padé coefficients $\{p_l\}_{l=0}^{L}$ and $\{q_m\}_{m=1}^{M}$ are calculated from the response $U_i(\omega)$. More details can be found in Refs. [18] and [17].

The velocity-to-force response matrix derived from Eq. (2) reads then

$$\mathbf{H}(\omega,\boldsymbol{\theta})=\mathrm{j}\omega[\mathbf{K}(\omega,\boldsymbol{\theta})-\omega^2\mathbf{M}]^{-1}, \tag{5}$$

which explicitly depends on the modulus parameters through the stiffness matrix, and whose generic element $H_{ij}(\omega,\boldsymbol{\theta})$ is the FRF relating the velocity at the ith dof to the force at the jth dof.

2.2. Experimental protocol

The setup of the single-input and single output is used for the ease of algorithmic illustration. All real structures are nonlinear to some extent. For a nonlinear system whose noise-free output is approximated by the Volterra series [19], at the kth frequency line

$$Y_0^{(\alpha)}(k)=\sum_{\alpha=1}^{\infty}Y_0^{(\alpha)}(k) \tag{6}$$

with $Y_0^{(\alpha)}(k)$ is the contribution of degree α. $Y_0^{(1)}(k)$ is the part corresponding to the underlying linear system, and $\sum_{\alpha=2}^{\infty}Y_0^{(\alpha)}$ is the contribution of the system nonlinearity. Under random excitations, $\sum_{\alpha=2}^{\infty}Y_0^{(\alpha)}$ can be split into two parts: one is the systematic bias due to the system nonlinearity, the other is the stochastic part $Y_S(k)$ which behaves like noise [20,21]. The former part along with the underlying linear system constitutes the related linear system $H_R(\omega_k)$. The modeling of the nonlinear system is shown Fig. 2, which is valid for a nonlinear structure whose output can be approximated by the

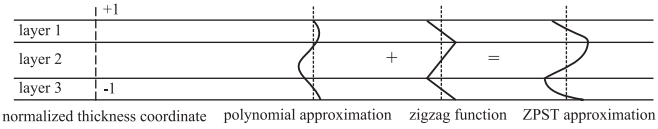

Fig. 1. ZPST displacement approximation.

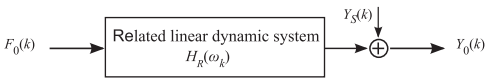

Fig. 2. Modeling of a nonlinear system under a normally distributed excitation. $F_0(k)$ and $Y_0(k)$ are the input–output noise-free spectra, $H_R(\omega_k)$ is the related underlying linear system, and $Y_S(k)$ represents the nonlinear distortions.

Volterra series in a mean square sense. Especially under the excitation of the random phase multisine (RPM), it can be proved – following the same lines as in Appendix 3A–3E of [20]—that $Y_S(k)$ is asymptotically a zero-mean circular complex normal variable. The RPM is defined as

$$q(t) = \sum_{k=1}^{n_\omega} A_k \sin\left(\frac{2k\pi}{T_p}t + \phi_k\right), \tag{7}$$

where the amplitudes $\{A_k\}_{k=1}^{n_\omega}$ are set uniform, and the phases $\{\phi_k\}_{k=1}^{n_\omega}$ are independent and identically distributed (i.i.d.) uniform variables in $[0,2\pi)$. By increasing the number of excited frequency lines (n_ω), the pdf of the RPM converges to be normal.

In the sequel, an experimental protocol is presented estimate $H_R(\omega_k)$ and quantify its uncertainty based on multiple experiments. Each experiment is controlled by a RPM of independent phase realization. In the rth experiment, the shaker is fed with the RPM of M_R periods. The application of the discrete Fourier transform to the pth period of the input–output observations yields

$$\begin{aligned} Y^{[p,r]}(k) &= H_R(\omega_k)F_0^{[r]}(k) + Y_S^{[r]}(k) + N_Y^{[p,r]}(k), \\ F^{[p,r]}(k) &= F_0^{[r]}(k) + N_F^{[p,r]}(k), \end{aligned} \tag{8}$$

where $N_F^{[p,r]}(k)$ and $N_Y^{[p,r]}(k)$ denote the input–output measurement noises, respectively. It is due to the application of the Fourier transform to the i.i.d. noises, $N_Y(k)$ and $N_F(k)$ become asymptotically circular normal variables and independent over frequencies according to the central limit theorem [22]. They account for the difference of the input–output spectra between periods so that the input–output measurement noises can be assessed by averaging over index p. From the noisy input–output spectra in (8), the sample means $\hat{Y}^{[r]}(k)$, $\hat{F}^{[r]}(k)$ and (co)variances $\hat{\sigma}^2_{\hat{Y}^{[r]}}(k)$, $\hat{\sigma}^2_{\hat{F}^{[r]}}(k)$ and $\hat{\sigma}^2_{\hat{Y}^{[r]}\hat{F}^{[r]}}(k)$ are computed. The FRF estimate $\hat{H}^{[r]}(\omega_k)$ is obtained using the maximum likelihood identification in an errors-in-variables framework, and its variance $\hat{\sigma}^2_{\hat{H}^{[r]}}(k)$ is derived from the sample (co)variances of the noises (see details in Appendix).

Prior to estimate the related linear system using multiple experiments, the denoised input–output spectra are projected onto the spectrum of the reference signal $q^{[r]}(t)$ in Eq. (7) to keep the phase synchronization,

$$\hat{Y}_q^{[r]}(k) = \hat{Y}^{[r]}(k)/Q^{[r]}(k), \quad \hat{F}_q^{[r]}(k) = \hat{F}^{[r]}(k)/Q^{[r]}(k). \tag{9}$$

These projections can now serve to estimate the related linear FRF following Appendix:

$$\hat{H}(\omega_k) = \hat{Y}(k)/\hat{F}(k), \tag{10}$$

where $\hat{F}(k)$ and $\hat{Y}(k)$ are the sample mean of $\{\hat{F}_q^{[r]}(k), \hat{Y}_q^{[r]}(k)\}_{r=1}^{M_R}$, respectively. The variance of $\hat{H}(\omega_k)$ is

$$\hat{\sigma}^2_{\hat{H}}(k) = |\hat{H}(\omega_k)|^2 \left\{ \frac{\hat{\sigma}^2_{\hat{Y}}(k)}{|\hat{Y}(k)|^2} + \frac{\hat{\sigma}^2_{\hat{F}}(k)}{|\hat{F}(k)|^2} - 2\,\mathrm{Re}\left[\frac{\hat{\sigma}^2_{\hat{Y}\hat{F}}(k)}{\hat{Y}(k)\overline{\hat{F}(k)}}\right] \right\}, \tag{11}$$

where $\overline{X}$ is the conjugate of a complex variable X, Re denotes the real part of a complex number, and $\hat{\sigma}^2_{\hat{Y}}(k)$, $\hat{\sigma}^2_{\hat{F}}(k)$ and $\hat{\sigma}^2_{\hat{Y}\hat{F}}(k)$ are the sample estimates of the (co)variances.

The variance $\hat{\sigma}^2_{\hat{H}}(k)$ is jointly compounded of the measurement noise and nonlinear distortions. The part due to the nonlinear distortions, $\hat{\sigma}^2_{\hat{H}_s}(k)$, can be separated out by assessing the difference

$$\hat{\sigma}^2_{\hat{H}_s}(k) = \hat{\sigma}^2_{\hat{H}}(k) - \hat{\sigma}^2_{\hat{H}_m}(k)/M_R \tag{12}$$

where $\hat{\sigma}^2_{\hat{H}_m}(k)$ denotes the sample mean of $\{\hat{\sigma}^2_{\hat{H}^{[r]}}(k)\}_{r=1}^{M_R}$ which are the variances contributed only by the measurement noise, and the factor M_R takes into account the averaging over realizations of the random phases.

3. Bayesian identification of the modulus parameters in the presence of measurement and modeling uncertainty

Effort is particularly focused on the construction of the surrogate model for the forward problem in Eq. (5) and on the hierarchical treatment of the modeling uncertainties.

3.1. Surrogate model

One of the principal advantages of the Bayesian approach is to deliver a marginal (or joint) pdf for the identified parameters. The pdf is usually not available in an explicit form. Often, sampling techniques like MCMC are used to explore the whole space of probability. However, a huge number of FE evaluations are required in the sampling process, which

makes this approach computationally expensive. In order to alleviate the Bayesian computation, a surrogate model is thus necessary to avoid time-consuming FE calculations. Various kinds of surrogate models exist, such as response surface model [23], polynomial chaos expansion [24], Kriging model [25]. An artificial neural network is advocated here as it can approximate arbitrary well any continuous function provided that the number of hidden units is sufficiently large and that the weights and biases are chosen appropriately [26].

3.1.1. Artificial neural network

A neural network is classically composed of a laminated architecture of neurons, with a first input layer ($\mathbf{x}$), intermediate layer(s) ($\mathbf{z}$), called hidden layer(s), and a final output layer ($\mathbf{y}$). Each layer is characterized by a different number of neurons, indicated by n_{inp}, n_{hid} and n_{out} for the input, hidden and output layers, respectively. The multilayer perception (one single hidden layer) is considered. The first layer of the network forms n_{hid} linear combinations of the inputs to give a set of intermediate activation variables

$$a_j^{(1)} = \sum_{i=1}^{n_{\text{inp}}} w_{ji}^{(1)} x_i + b_j^{(1)}, \quad j = 1, \ldots, n_{\text{hid}} \tag{13}$$

with each variable $a_j^{(1)}$ associated with each hidden unit. $w_{ji}^{(1)}$ represents the connection weight and $b_j^{(1)}$ is the bias parameter associated with the hidden unit. $\{a_j^{(1)}\}_{j=1}^{n_{\text{hid}}}$ are transformed through a nonlinear activation function of the hidden layer,

$$z_j = f^{(1)}[a_j^{(1)}], \quad j = 1, \ldots, n_{\text{hid}} \tag{14}$$

$\{z_j\}_{j=1}^{n_{\text{hid}}}$ are then transformed to the second layer activation values

$$a_k^{(2)} = \sum_{j=1}^{n_{\text{hid}}} w_{kj}^{(2)} z_j + b_k^{(2)}, \quad k = 1, \ldots, n_{\text{out}} \tag{15}$$

Finally, $\{a_k^{(2)}\}_{k=1}^{n_{\text{out}}}$ are passed through the output-unit activation function to deliver output values $y_k = f^{(2)}[a_k^{(2)}], k = 1, \ldots, n_{\text{out}}$. The connection weights and biases in Eqs. (13)–(15) are in fact the parameters of the surrogate model which have to be adapted through a supervised training procedure by means of the error back-propagation algorithm [27].

3.1.2. Sampling plan and prior probability density functions

In order to train the neural network, an experiment plan is designed in the parameter space to generate sample data using the efficient Latin Hypercube Sampling (LHS) method. To this end, a pdf is first defined for each parameter, based on the maximum entropy principle [28] from theoretical or engineering results. Prior information on the Young's modulus of a polymer is often available, or can be measured with a preliminary dynamical mechanical analysis test. Based on the limited available information (single value, positivity), a truncated normal pdf or a Gamma pdf can be reasonably chosen as a prior according to the maximum entropy principle, e.g. the relaxation time τ follows a Gamma distribution $\Gamma(k_\tau, \beta_\tau)$

$$\pi(\tau | k_\tau, \beta_\tau) \propto \frac{1}{\beta_\tau^k (k_\tau - 1)!} \tau^{(k_\tau - 1)} \exp\left(-\frac{\tau}{\beta_\tau}\right), \tag{16}$$

where $\propto$ means "is proportional to", k_τ is the shape parameter of positive-integer value, and β_τ is the scale parameter.

The coupling between μ and ν in Eq. (1) gives an additional constraint: $\mu \geq \nu$. Such constraint is equivalent to $\nu = \mu - \epsilon$ with $\epsilon \notin \mathcal{R}^-$. The random variable ϵ replaces ν to constitute the vector $\boldsymbol{\theta}$, whose elements can be seen as mutually independent from a prior point of view; this simplifies the construction of the joint prior pdf.

3.1.3. Approximation of the frequency response function by a rational form

Using the sample data $\{\boldsymbol{\theta}_i\}_{i=1}^{n_s}$, the FRFs are calculated, which take values at numerous frequencies. The behavior of each FRF around the poles can be very different according to the tested parameters. As a result, it seems difficult to link directly the parameters $\boldsymbol{\theta}$ to the FRFs by a neural network with a limited number of layers. One possible way is to project the FRFs onto a rational basis functions, and make the connection between the projected coefficients and $\boldsymbol{\theta}$.

According to the Mittag–Leffler theorem [29], any transfer function can be expanded in an infinite sum of partial fractions. Since the active frequency range of each partial fraction is limited, the FRF in Eq. (5) can be well approximated with a rational form of finite order in a particular frequency band of interest,

$$H(\omega, \boldsymbol{\lambda}, \mathbf{c}, e_d, e_s) = \sum_{k=1}^{n_m} \left(\frac{\mathcal{A}_k}{\mathrm{j}\omega - \lambda_k} + \frac{\overline{\mathcal{A}}_k}{\mathrm{j}\omega - \overline{\lambda}_k} \right) + \mathrm{j}\omega e_d + e_s, \tag{17}$$

where n_m is the model order (twice the number of poles), $\lambda_k = -\eta_k \omega_{0k} + \mathrm{j}\sqrt{1-\eta_k^2}\,\omega_{0k}$ with ω_{0k} the natural frequency and η_k the damping ratio, $\mathcal{A}_k$ is the pole residue, and e_s, $\mathrm{j}\omega e_d$ represent the static and dynamic terms to model the influence of the nearest poles outside the frequency range. These modal parameters, concatenated in $\boldsymbol{\alpha}$, can be extracted by using a maximum likelihood identification [20] or a vector-fitting technique [30].

The key step to extract accurately $\boldsymbol{\alpha}$ lies in the choice of an appropriate frequency band in which the modes of the FRFs are fully covered. At a first glance, it appears impossible to determine a unique frequency band with the same number of poles for all the realizations $\{\mathbf{H}_i\}_{i=1}^{n_s}$. Nevertheless, the FRFs can be grouped according to their similarity (having the same poles) by clustering techniques, a same frequency band being then determined for each class. The grouping of the FRFs can be achieved by means of the k-means clustering technique, or in a more sophisticated way it is obtained from the mixture of probabilistic principal component analysis by maximizing the log-likelihood

$$l(\mathbf{z},\mathbf{x},\mathbf{u},\mathbf{W},\boldsymbol{\sigma}) = \sum_{k=1}^{n_s} \log\left[\sum_{i=1}^{n_{\text{cluster}}} \pi(z_k=i)\pi(\mathbf{H}_k|z_k=i)\right], \tag{18}$$

where z is the variable labeling the FRF, $\pi(z_k=i)$ is the corresponding mixing portion of the ith class, and $\pi(\mathbf{H}_k|z_k=i)$ denotes the probability that $\mathbf{H}_k$ belongs to the ith class. The class label variables $\{z_k\}_{z_k=1}^{n_s}$ are tuned by the expectation-maximization algorithm [31], they provide a robust partition of the FRFs (with a complex data structure).

Finally, the whole process of the surrogate model's construction is displayed in Fig. 3.

3.2. Formulation of the Bayesian parameter identification

In this section, parameter estimation is formulated with the consideration of the measurement and modeling uncertainties. The assessment of the nonmodeled dynamics is obviously a much more difficult task since, by definition, it is out of reach. The probabilistic approach followed in the present work views the nonmodeled dynamics as random via the epistemic uncertainty (due to the lack of knowledge). The random variables describing the modeling uncertainty, denoted by $\boldsymbol{\gamma}$, are to be inferred jointly with the modulus identification.

In the current configuration, the unknown variables include the Young's modulus parameters $\boldsymbol{\theta}$ and the random variables $\boldsymbol{\gamma}$ characterizing the modeling uncertainty, which are updated through the Bayes' rule

$$\pi(\boldsymbol{\theta},\boldsymbol{\gamma}|\mathcal{D}) \propto \pi(\mathcal{D}|\boldsymbol{\theta},\boldsymbol{\gamma})\pi(\boldsymbol{\theta},\boldsymbol{\gamma}), \tag{19}$$

where $\pi(\mathcal{D}|\boldsymbol{\theta},\boldsymbol{\gamma})$ is the likelihood function of the measurement data $\mathcal{D}$ given the values of $\{\boldsymbol{\theta},\boldsymbol{\gamma}\}$, and $\pi(\boldsymbol{\theta},\boldsymbol{\gamma})$ is the prior pdf which is assumed to be factorisable, $\pi(\boldsymbol{\theta},\boldsymbol{\gamma}) = \pi(\boldsymbol{\theta})\pi(\boldsymbol{\gamma})$.

The assigned prior pdf should be rather flat, which reflects the lack of precise information, in order to avoid $\pi(\boldsymbol{\theta},\boldsymbol{\gamma}|\mathcal{D})$ to be dominated by the (probably subjective) prior information. Attention should also be paid when the pdf of a truncated form is used, for its support must cover all possible values.

3.3. Likelihood function

The likelihood function is formulated based on the modal data, the pdf's of the modal data, embodying the measurement and modeling uncertainties, are required. The uncertainty of the FRF due to the measurement noise and nonlinear distortions has been shown to be circular complex normally distributed; it can be propagated to the modal parameters by applying a Monte Carlo procedure. A set of samples $\mathcal{D} = \{\boldsymbol{\alpha}_{\text{exp}}^{(i)}\}_{i=1}^{n_{\boldsymbol{\alpha}}}$ are obtained using the vector fitting technique, and $\boldsymbol{\alpha}_{\text{exp}}$ denotes the experimental modal parameters. The distribution of the sample mean $\hat{\boldsymbol{\alpha}}$ tends to be normal according to the central limit theorem as $n_{\boldsymbol{\alpha}}$ becomes large

$$\pi(\hat{\boldsymbol{\alpha}}-\boldsymbol{\alpha}_0) = \mathcal{N}(\mathbf{0},\mathbf{C}_{\text{exp}}), \tag{20}$$

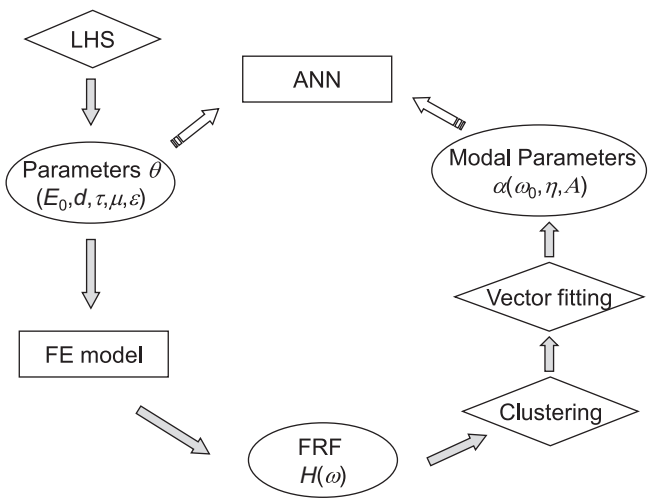

Fig. 3. Schema of the surrogate model's construction.

where $\boldsymbol{\alpha}_0$ represents the modal parameters of the related linear system, and $\mathbf{C}_{\text{exp}}$ is the covariance matrix of the sample mean $\hat{\boldsymbol{\alpha}}$

$$\mathbf{C}_{\text{exp}} = \frac{1}{n_{\boldsymbol{\alpha}}(n_{\boldsymbol{\alpha}}-1)} \sum_{i=1}^{n_{\boldsymbol{\alpha}}} [\boldsymbol{\alpha}_{\text{exp}}^{(i)} - \hat{\boldsymbol{\alpha}}][\boldsymbol{\alpha}_{\text{exp}}^{(i)} - \hat{\boldsymbol{\alpha}}]^T, \tag{21}$$

with T the transpose operator.

On the other hand, the pdf of the modeling uncertainty must be defined. However, any probabilistic assumption can at most cover one part of the nonmodeled dynamics. The approach followed in the present work is to describe the modeling error by a zero-mean multivariate normal pdf,

$$\pi[\boldsymbol{\alpha}_0 - \boldsymbol{\alpha}(\boldsymbol{\theta})] = \mathcal{N}(\mathbf{0}, \mathbf{C}_{\text{mod}}), \tag{22}$$

where $\mathbf{C}_{\text{mod}}$ is an unknown covariance matrix. It is composed of three diagonal block matrices

$$\mathbf{C}_{\text{mod}}^{\boldsymbol{\omega}} = \gamma_{\boldsymbol{\omega}} \boldsymbol{\Lambda}_{\omega},\ \mathbf{C}_{\text{mod}}^{\boldsymbol{\eta}} = \gamma_{\boldsymbol{\eta}} \boldsymbol{\Lambda}_{\eta},\ \mathbf{C}_{\text{mod}}^{\mathcal{A}} = \gamma_{\mathcal{A}} \boldsymbol{\Lambda}_{\mathcal{A}}, \tag{23}$$

where each block consists of a predefined structure and a weighting coefficient. The diagonal elements of the used-chosen $\boldsymbol{\Lambda}$ are defined as the square values of the sample means $\hat{\boldsymbol{\alpha}}$, e.g. $\boldsymbol{\Lambda}_{\omega} = \text{diag}(\hat{\omega}_1^2, \ldots, \hat{\omega}_{n_m}^2)$, similarly for $\boldsymbol{\Lambda}_{\eta}$ and $\boldsymbol{\Lambda}_{\mathcal{A}}$. This choice is in accordance with the cost function, defined as a weighted relative residual like $\sum_i \gamma_i [1 - f_i(\boldsymbol{\theta})/\hat{f}_i]^2$, used in numerous optimization cases for parameter identification for instance in Refs. [7,8,32] with $\{\gamma_i\}$ determined by the prior belief. Instead of being set by the user, the weighting coefficients $\gamma_{\boldsymbol{\omega}}$, $\gamma_{\boldsymbol{\eta}}$ and $\gamma_{\boldsymbol{\mathcal{A}}}$, constituting the vector $\boldsymbol{\gamma}$, have to be tuned jointly with the modulus parameters $\boldsymbol{\theta}$ from the measurements.

By considering the measurement noise, the nonlinear distortions and the modeling uncertainties, the likelihood function in Eq. (19) of the experimental modal data $\boldsymbol{\alpha}$ given the values of the parameters $\boldsymbol{\theta}$ and $\boldsymbol{\gamma}$ is formulated as follows:

$$\begin{aligned} \pi(\mathcal{D}|\boldsymbol{\theta},\boldsymbol{\gamma}) &= \int \pi(\hat{\boldsymbol{\alpha}}|\boldsymbol{\alpha}_0)\pi[\boldsymbol{\alpha}_0|\boldsymbol{\alpha}(\boldsymbol{\theta}),\boldsymbol{\gamma}]\, \mathrm{d}\boldsymbol{\alpha}_0 \\ &\propto |\mathbf{C}_{\boldsymbol{\alpha}}(\boldsymbol{\gamma})|^{-1} \exp\left\{-\frac{1}{2}[\hat{\boldsymbol{\alpha}} - \boldsymbol{\alpha}(\boldsymbol{\theta})]^T \mathbf{C}_{\boldsymbol{\alpha}}^{-1}(\boldsymbol{\gamma})[\hat{\boldsymbol{\alpha}} - \boldsymbol{\alpha}(\boldsymbol{\theta})]\right\} \end{aligned} \tag{24}$$

with $\mathbf{C}_{\boldsymbol{\alpha}}(\boldsymbol{\gamma}) = \mathbf{C}_{\text{exp}} + \mathbf{C}_{\text{mod}}(\boldsymbol{\gamma})$. It is observed that most of error sources are explicitly involved in the Bayesian formulation for parameter estimation, the modeling uncertainty is taken into account through an assigned parametric model.

It is worth noting that Eq. (24) gives a general way to take into account the measurement and modeling uncertainties. The former, carried in $\pi(\hat{\boldsymbol{\alpha}}|\boldsymbol{\alpha}_0)$ in Eq. (20), is shown to asymptotically follow a Gaussian pdf by means of the central limit theorem. The probabilistic modeling error is expected to be zero-mean for a sophisticated numerical model, the choice of a Gaussian form being motivated by making feasible and efficient the computation of the convolution involved in Eq. (24). In addition, this is in accordance with the maximum entropy principle.

It should be also mentioned that the mechanical/geometrical properties of the external layers and experiment setting (e.g. shaker position) are assumed to be precise with negligible uncertainties. In fact, their parametric uncertainties can be incorporated into the Bayesian parameter estimation by assigning them appropriate probability distributions.

3.4. Hierarchical modeling of the weighting coefficients

The joint identification of the modulus parameters $\boldsymbol{\theta}$ and the weighting coefficients $\boldsymbol{\gamma}$ based on Eq. (24) can lead to an ill-conditioned case, since increasing the weighting coefficients $\boldsymbol{\gamma}$ might always favor the increase of the likelihood of the experimental data. Prior information should thus be assigned to $\boldsymbol{\gamma}$ to regularize the joint parameter identification. Each element of $\boldsymbol{\gamma}$ follows a prior Gamma pdf $\Gamma(k_{\gamma},\beta)$, whose mean value, say $k_{\gamma}\beta$, suggests the one's prior belief on the level of the modeling uncertainty (an approximate percentage of the absolute value of a modal parameter, see the definition in Eq. (23)). The shape parameter k_{γ} is set small so that the distribution can have a long tail, i.e. a wide support, to cover all the possible values of the weighting coefficients. The scale parameter β remains then to be determined.

However, assigning a value to β by a prior belief is not straightforward and may have a significant influence on the posterior pdf of the weighting coefficients, consequently on the modulus identification. Therefore, it is better to treat β as an uncertain variable and tune it by the Bayesian inference. Within the Bayesian context, β is a so-called hyper-parameter, here it follows a Gamma pdf $\Gamma(k_{\beta},\beta_0)$, where k_{β} and β_0 are known *a priori*. The above probabilistic modeling of the weighting coefficients constitutes a hierarchical Bayes model [9]

$$(k_{\beta},\beta_0) \underbrace{\longrightarrow}_{\pi(\beta|k_{\beta},\beta_0)} \beta \underbrace{\longrightarrow}_{\pi(\boldsymbol{\gamma}|k_{\gamma},\beta)} (\gamma_{\omega},\gamma_{\eta},\gamma_{\mathcal{A}}) \tag{25}$$

The Bayesian hierarchical modeling allows incorporating the prior information (soft constraint) to avoid the potential degeneracy (due to the joint identification of parameters of different kinds), it can also make robust the identification results with respect to the choice of the prior information by virtue of the hierarchical modeling of the weighting coefficients.

3.5. Bayesian parameter learning in conjunction with Markov Chain Monte Carlo

The application of the Bayes's rule to all the unknown variables delivers the posterior pdf (up to a constant)

$$\pi(\boldsymbol{\theta},\boldsymbol{\gamma},\beta|\mathcal{D}) \propto l(\mathcal{D}|\boldsymbol{\theta},\boldsymbol{\gamma})\pi(\boldsymbol{\theta})\pi(\boldsymbol{\gamma}|\beta)\pi(\beta), \tag{26}$$

which is the full solution of the Bayesian approach, and carries much more information than a point estimate provided by most of the classical estimation methods. Often, the posterior $\pi(\boldsymbol{\theta},\boldsymbol{\gamma},\beta|\mathcal{D})$ is a complex and implicit function of the parameters, which is difficult to explore as such. Sampling techniques, such as MCMC, should be used as it can avoid calculating the normalization constant and draw samples directly from $\pi(\boldsymbol{\theta},\boldsymbol{\gamma},\beta|\mathcal{D})$. The principle of MCMC consists in generating a sequence of random walks whose stationary distribution coincides with the posterior pdf [33,34].

On account of the high complexity of $\pi(\boldsymbol{\theta},\boldsymbol{\gamma},\beta|\mathcal{D})$, such as strong correlation between the parameters, a simple MCMC like Metropolis–Hastings algorithm explores quite slowly the whole posterior space due to high rejection rate of the candidate samples. To accelerate the exploration of a pdf, one effective solution is to use a population of Markov chains where the stochastic walk is based on a set of search points. During the sampling process, the population is evolved by mutation (Metropolis update in a single chain), crossover (partial states swapping between different chains) and exchange operators (full state swapping between adjacent chains). The MCMC sampler constructed in such a way bears a high similarity with genetic algorithms [35–37]. In the followings, a brief view is given to understand how it deals with complex pdf's:

- A stochastic search starts with a population of points randomly placed at different locations in the parameter space, which provides a natural way to accelerate the exploration of the probability space of parameters, even in a case of multimode.
- The diversity of the population plays a crucial role in maintaining the efficiency of the stochastic algorithm. This can be realized by invoking parallel tempering which works by simulating a sequence of distributions along a temperature ladder [38]. Simulations at high temperature levels help the system to overcome the barriers of energy landscapes. Rewriting $\pi(\boldsymbol{\theta},\boldsymbol{\gamma},\beta|\mathcal{D})$ in an exponential form $\exp[-\Delta(\boldsymbol{\theta},\boldsymbol{\gamma},\beta)]$, a sequence of pdf's is defined in the following way:
$$\pi_l(\boldsymbol{\theta},\boldsymbol{\gamma},\beta|\mathcal{D}) = z(t_l)\exp[-\Delta(\boldsymbol{\theta},\boldsymbol{\gamma},\beta)/t_l], \quad l=1,\ldots,n_c \tag{27}$$
with $z(t_l)$ the normalization constant and n_c the number of Markov chains. The temperatures $1=t_1<,\cdots,<t_{n_c}$ create a ladder, each temperature is associated with a target distribution toward which the corresponding Markov chain converges. t_1 corresponds to the posterior pdf of interest.
- The exchange of information between two samples running in parallel is seen as a way to improve the performance of the MCMC sampler, such as rapid mixing, which is realized through the cross and swap operators. The states of adjacent chains swap with a probability according to the Metropolis–Hasting criterion. A sample with a weak fitness value will climb up the temperature ladder and will probably be eliminated as mutation operations (e.g. random walks) are accepted with a higher probability at high temperatures. On the contrary, a sample with a high fitness value will climb down the temperature ladder and will probably be stored as mutation operations are accepted with a lower probability at low temperatures.

The enriched MCMC method has therefore the learning capability of a genetic algorithm as well as the fast mixing ability of parallel tempering, which explains its good performances in dealing with complex pdf's. From the samples of $\boldsymbol{\theta}$ returned by MCMC, the pdf of the elastic modulus can be estimated at each frequency by using the kernel density estimation [39].

4. Experimental applications

The proposed approach is illustrated on the estimation of the Young's modulus of a polyvinyl butyric (PVB) layer in laminated glass. Two kinds of laminated glasses are considered, one is made with a classical PVB polymer in the interlayer, the other is made with a specific PVB polymer with a high damping. The laminated glass samples are 0.6 m long and 0.025 m wide. Other geometrical and mechanical properties are presented in Table 1.

The beam is modeled with the ZPST shell element, and meshed with 4 elements in width and 100 elements in length. The coarse frequency grid [80, 220, 500, 950, 1500, 2200, 3200, 4500, 5800] (unity: Hz) is set quite dense for the Padé approximation, based on which the Padé reconstruction is guaranteed to be always valid for all the FRFs in the frequency range of interest. To construct the surrogate model, $n_s = 2\times10^4$ samples are generated by a truncated LHS based on

Table 1
Physical properties of the laminated glass. (1) standard PVB, (2) modified PVB.

Material	Thickness ($\times10^{-3}$ m)	Density (kg m^{-3})	Poisson ratio	Elastic modulus (Pa)
Glass	3.8	2500	0.22	72×10^9
Polymer	$0.76^{(1)}$, $0.86^{(2)}$	900	0.49	To be identified

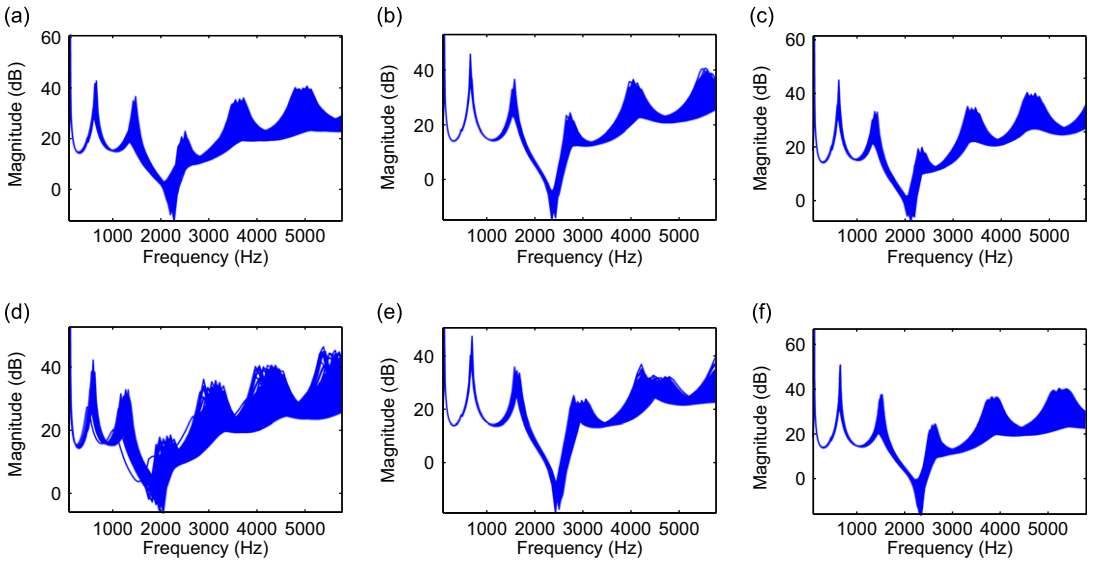

Fig. 4. Clustered frequency response functions, $n_{\text{cluster}} = 6$.

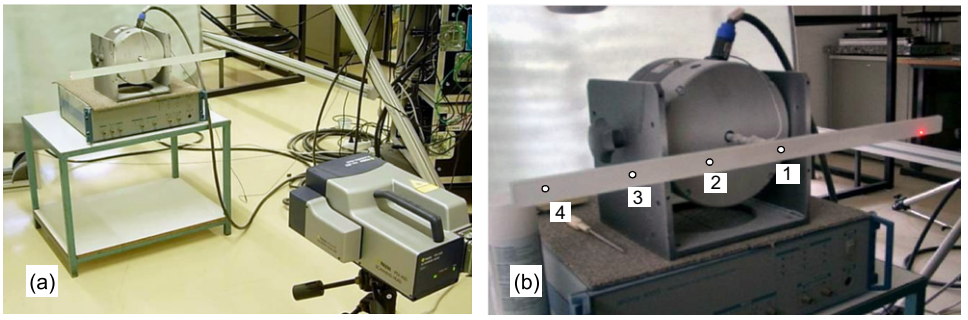

Fig. 5. Experimental set up, as described in the ISO standard [40].

a rather flat prior pdf of $\boldsymbol{\theta}$. The computed FRFs are clustered into 6 classes shown in Fig. 4, for each of which an appropriate frequency band is chosen for modal parameter estimation. At the end, a multilayer perception neural network is applied to link the parameters $\boldsymbol{\theta}$ with the modal parameters $\boldsymbol{\alpha}$.

Fig. 5 illustrates the experimental configuration proposed in the ISO standard [40]. The laminated glass beam is excited at its center (point 1) by a shaker; the impedance head, coupled to a shaker, is connected to the beam with the aid of an impact button.

The sampling frequency is set as $f_s = 16{,}384$ Hz. A RPM with uniform amplitude is applied to the shaker with $M_P = 32$ periods and $M_R = 30$ phase realizations. The vibration velocities at three observed locations (points 2, 3 and 4) are measured by a Laser Doppler vibrometer in a thermostatic chamber with $T_{\text{ref}} = 21.5\ ^\circ\text{C}$. The first two periods of the measured signals are ignored to reduce the transient effect. Three estimated FRFs are displayed with their variances due to the measurement noise and the nonlinear distortions in Fig. 6.

A prior Gamma distribution $\Gamma(k_\beta, \beta_0)$ of β is set with $k_\beta = 2$ and $\beta_0 = 10^{-4}$. The assigned values correspond to a modeling uncertainty's level around 1 percent of the absolute true values of the modal parameters. 3×10^4 samples are drawn from the posterior distribution $\pi(\boldsymbol{\theta}, \boldsymbol{\gamma}, \beta | \mathcal{D})$ by running the MCMC method with a population size $n_c = 200$. In principle, any kind of statistics can be computed for the updated parameters based on these samples. The posterior pdf's of the modulus parameters are illustrated in Fig. 7 in comparison with the prior ones. The pdf of each parameter becomes narrower by fusing the experimental information with the prior information. These pdf's embody the uncertainty originating from the measurement and modeling uncertainties. The pdf's of the estimated real part (storage modulus), imaginary part (loss modulus) and Tangent delta of the Young's modulus are presented in Fig. 8 for the beam with standard PVB. The resulting Young's modulus estimate is less reliable at high frequencies where the fractional derivative model is more sensible to the variation of the Young's modulus through the parameters $\boldsymbol{\theta}$. Fig. 9 shows a good agreement between the FRFs computed with the optimal posterior modulus and the experimental ones in terms of magnitude and phase.

Likewise, Fig. 10 presents the pdf's of the modulus identified for the beam with the modified PVB. The FRFs calculated with the optimal prior and posterior Young's moduli are displayed in comparison with the experimental ones in Fig. 11.

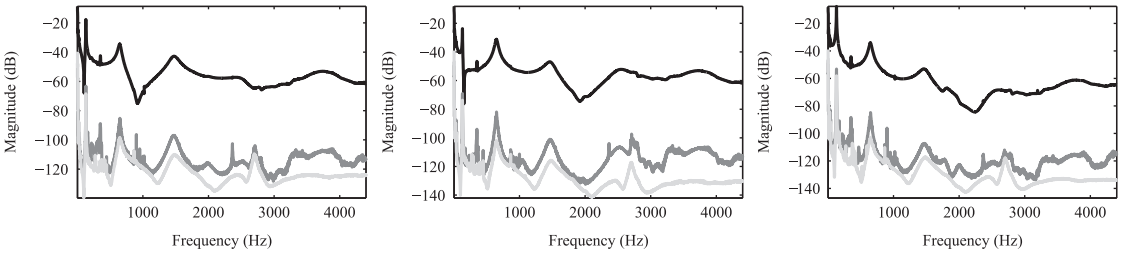

Fig. 6. FRF measurements realized at three different points on the laminated sample with a core layer made of standard PVB. ▬ FRF, ▬ standard deviations of nonlinear distortions, ▬ standard deviations of measurement noise.

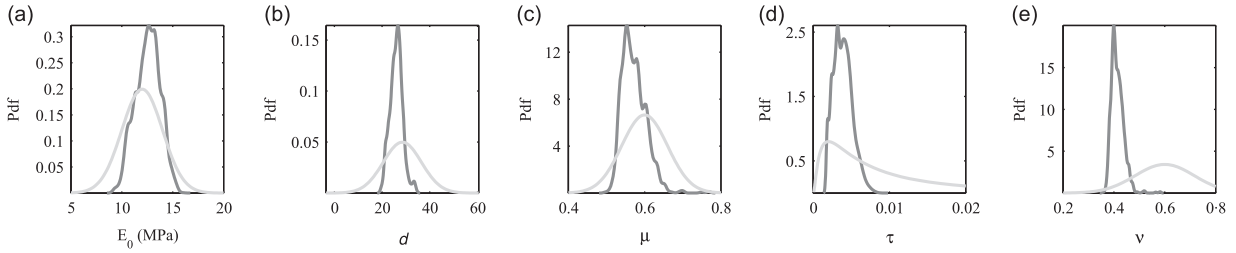

Fig. 7. Probability density functions of the modulus parameters in the case of standard laminated glass, ▬ Prior pdf, ▬ Posterior pdf.

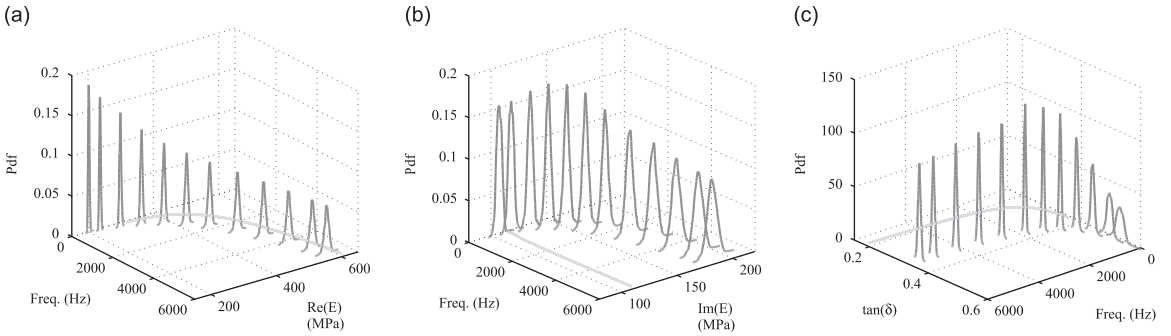

Fig. 8. From left to right: Real part, Imaginary part, and Tangent delta of the Young's modulus for the standard laminated glass, ▬ Posterior probability density functions, ▬ Prior nominal values.

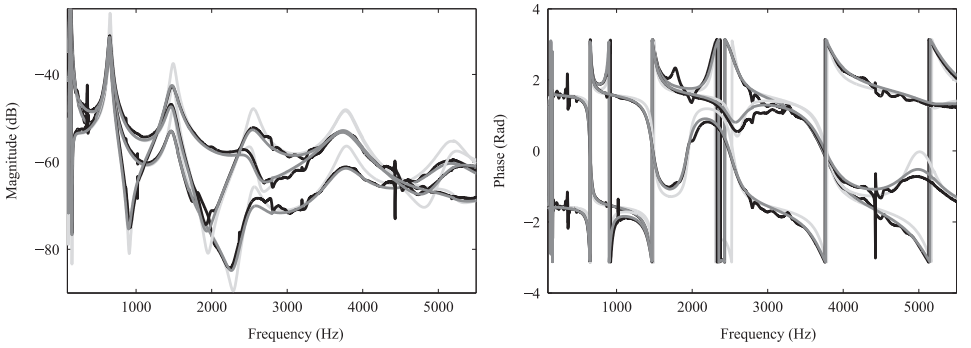

Fig. 9. Frequency response functions for the standard laminated glass in magnitude (left), and phase (right). ▬ Measured FRFs, ▬ Posterior FRFs, ▬ Prior FRFs.

The weighting coefficients tuned jointly with the modulus are shown in Fig. 12. The updated weighting coefficients do not have the same level especially for γ_A which is associated with the mode shapes. Such imperfect agreement can be understood by the following facts: (1) the numerical model is not sufficient to capture the full dynamics of the sandwich beam especially at high frequencies due to the complex behavior of the (not really homogeneous) PVB layer and (2) the measurement is perturbed (low signal-to-noise ratio) at high frequencies, as reflected in Fig. 11.

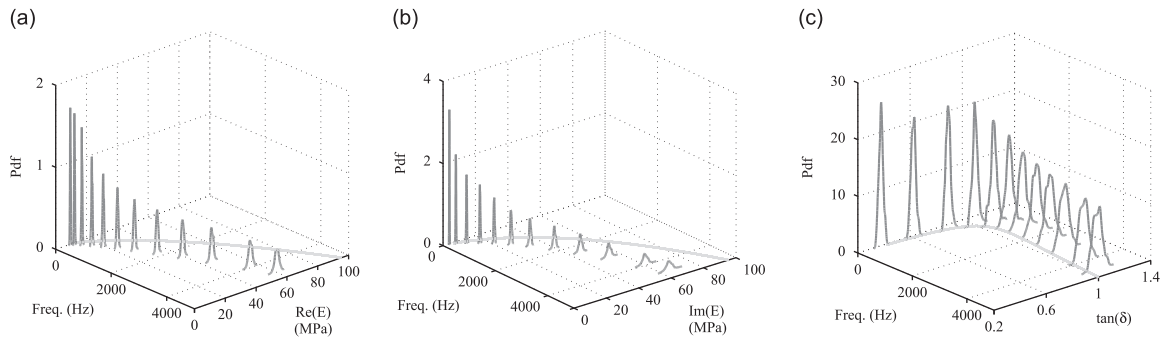

Fig. 10. From left to right: Real part, Imaginary part, and Tangent delta of the Young's modulus for the modified laminated glass, ▬ Posterior probability density functions, ▬ Prior nominal values.

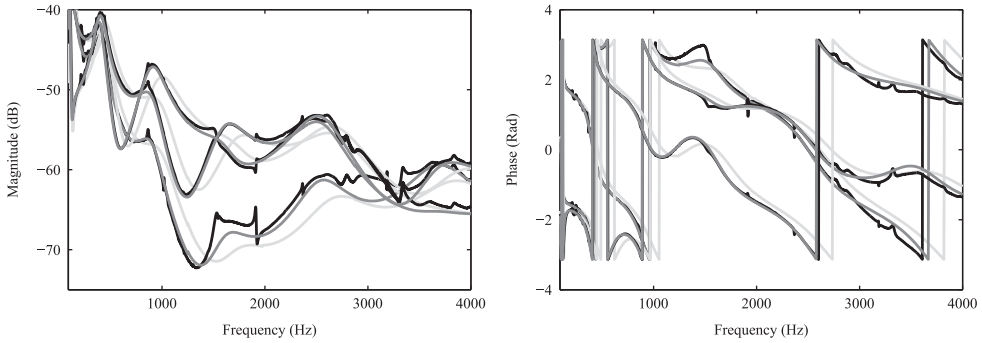

Fig. 11. Frequency response functions for the modified laminated glass in magnitude (left), and phase (right). ▬ Measured FRFs, ▬ Posterior FRFs, ▬ Prior FRFs.

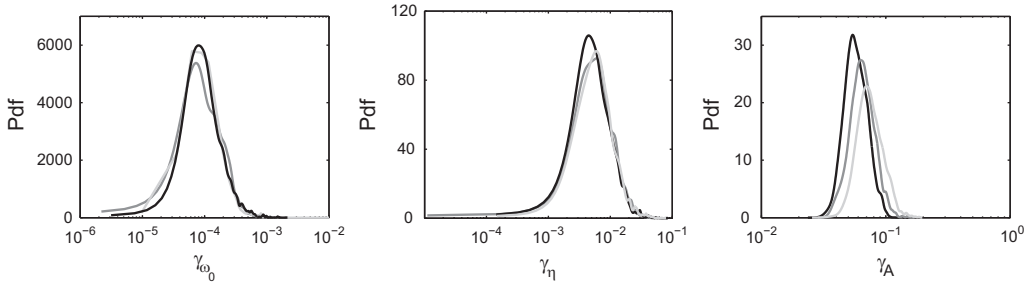

Fig. 12. Probability density functions of the weighting coefficients in the case of the modified laminated glass, ▬ $\beta_0 = 10^{-6}$, ▬ $\beta_0 = 10^{-4}$, ▬ $\beta_0 = 10^{-2}$.

Fig. 12 illustrates the influence on the estimates of the weighting coefficients by using different prior information. It is observed that the pdf's of γ share the dominant probability mass for $\beta_0 = 10^{-6}$, 10^{-4} and 10^{-2}, respectively. It is verified by experimental applications that due to the hierarchical modeling strategy, the choice of the prior information on the modeling uncertainty is no more critical to obtain a reliable identification.

5. Conclusion

A complete probabilistic Bayesian approach for identifying the frequency-dependent Young's modulus of the viscoelastic material in a laminated structure has been presented in the presence of errors from various origins, with application to laminated glasses. One of its main advantages stands in its capacity to return the quantified uncertainty in the form of posterior probability density function for the Young's modulus. The Bayesian Young's modulus identification is based on a layered finite element model and a specific experimental protocol, whose efficiency strongly relies on the proposed combination of a surrogate model and a Markov Chain Monte Carlo sampler.

Acknowledgments

The authors acknowledge the financial support from the project Vermetal within the framework of i-Trans competitiveness cluster in France. The authors would like to thank Profs. Rik Pintelon and Johan Schoukens at VUB for their guidance in design of experiment protocol use the random phase multisine.

Appendix A

The measurement of FRF falls into the errors-in-variables framework, in which the input and output are both contaminated by additive measurement errors. At the kth frequency line

$$F^{[r,p]}(k) = F_0^{[r]}(k) + N_F^{[r,p]}(k) \tag{28}$$

$$Y^{[r,p]}(k) = Y_0^{[r]}(k) + N_Y^{[r,p]}(k) \tag{29}$$

with $Y_0^{[r]}(k) = H_0^{[r]}(\omega_k) F_0^{[r]}(k)$. The unknown variable are the input–output noise-free spectra $F_0^{[r]}(k)$, $Y_0^{[r]}(k)$, and $H_0^{[r]}(\omega_k)$. A maximum likelihood formulation is used to estimate them from noisy input–output observations $\{F^{[r,p]}(k), Y^{[r,p]}(k)\}_{p=1}^{M_P}$,

$$\min_{H_0^{[r]}(\omega_k), Y_0^{[r]}(k), F_0^{[r]}(k)} \left|Y^{[r]}(k) - Y_0^{[r]}(k)\right|^2 \sigma_{Y^{[r]}}^{-2} + \left|F^{[r]}(k) - F_0^{[r]}(k)\right|^2 \sigma_{F^{[r]}}^{-2} \tag{30}$$

with the constraint $Y_0^{[r]}(k) - H_0^{[r]}(\omega_k) F_0^{[r]}(k) = 0$. By introducing a Lagrange multiplier λ, it is converted into

$$\min_{H_0^{[r]}(\omega_k), Y_0^{[r]}(k), F_0^{[r]}(k)} \left|Y^{[r]}(k) - Y_0^{[r]}(k)\right|^2 \sigma_{Y^{[r]}}^{-2} + \left|F^{[r]}(k) - F_0^{[r]}(k)\right|^2 \sigma_{F^{[r]}}^{-2} + \lambda [Y_0^{[r]}(k) - H_0^{[r]}(\omega_k) F_0^{[r]}(k)] \tag{31}$$

By setting to zero the first-order derivatives of the cost function with respect to all the unknown variables, it follows that

$$\hat{H}^{[r]}(\omega_k) = \frac{\hat{Y}^{[r]}(k)}{\hat{F}^{[r]}(k)} = \frac{\frac{1}{M_P}\sum_{p=1}^{M_P} \hat{Y}^{[r,p]}(k)}{\frac{1}{M_P}\sum_{p=1}^{M_P} \hat{F}^{[r,p]}(k)} \tag{32}$$

with $\hat{H}^{[r]}(\omega_k)$, $\hat{Y}^{[r]}(k)$ and $\hat{F}^{[r]}(k)$ the estimates of $H_0^{[r]}(\omega_k)$, $Y_0^{[r]}(k)$ and $F_0^{[r]}(k)$.

Writing the estimates of the input–output spectra as the true values plus the additive errors, and further applying the first-order Taylor expansion yields

$$\begin{aligned} \hat{H}^{[r]}(\omega_k) &= \frac{\hat{Y}^{[r]}(k)}{\hat{F}^{[r]}(k)} = \frac{Y_0^{[r]}(k) + \hat{N}_Y^{[r]}(k)}{F_0^{[r]}(k) + \hat{N}_F^{[r]}(k)} \\ &= H_0^{[r]}(\omega_k) \frac{1 + \frac{\hat{N}_Y^{[r]}(k)}{Y_0^{[r]}(k)}}{1 + \frac{\hat{N}_U^{[r]}(k)}{F_0^{[r]}(k)}} \approx H_0^{[r]}(\omega_k) \left[1 + \frac{\hat{N}_Y^{[r]}(k)}{Y_0^{[r]}(k)} - \frac{\hat{N}_F^{[r]}(k)}{F_0^{[r]}(k)}\right] \end{aligned} \tag{33}$$

The deviation $\hat{H}^{[r]}(\omega_k) - H_0^{[r]}(\omega_k)$ is a zero mean complex normally distributed variable, the variance of the FRF estimate is directly computed based on Eq. (33).

References

[1] A. Nashif, D. Jones, J. Henderson, *Vibration Damping*, Wiley-Interscience, New York, 1985.
[2] A.S.E. 1876-99, *Standard Test Method for Dynamic Young's Modulus, Shear Modulus, and Poisson's Ratio by Impulse Excitation of Vibration, Annual Book of ASTM Standards*, American Society for Testing and Materials, West Conshohocken, PA, 1999.
[3] R. Pintelon, P. Guillaume, S. Vanlanduit, K. De Belder, Y. Rolain, Identification of Young's modulus from broadband modal analysis experiments, *Mechanical Systems and Signal Processing* 18 (2004) 699–726.
[4] E. Barkanov, E. Skukis, M. Wesolowski, A. Chate, Characterization of adhesive layers in sandwich composites by nondestructive technique, *International Journal of Aerospace and Mechanical Engineering* 4 (2010) 1–6.
[5] S.Y. Kim, D.H. Lee, Identification of fractional-derivative-model parameters of viscoelastic materials from measured FRFs, *Journal of Sound and Vibration* 324 (2009) 570–586.
[6] D.A. Castello, F.A. Rochinha, N. Roitman, C. Magluta, Constitutive parameter estimation of a viscoelastic model with internal variables, *Mechanical Systems and Signal Processing* 22 (2008) 1840–1857.
[7] M. Martinez-Agirre, M.J. Elejabarrieta, Dynamic characterization of high damping viscoelastic materials from vibration test data, *Journal of Sound and Vibration* 330 (2011) 3930–3943.
[8] A. Renault, L. Jaouen, F. Sgard, Characterization of elastic parameters of acoustical porous materials from beam bending vibrations, *Journal of Sound and Vibration* 330 (2011) 1950–1963.
[9] P. Lee, *Bayesian Statistics*: *An Introduction*, Arnold Press, London, 1997.
[10] A. Tarantola, *Inverse Problem Theory and Methods for Model Parameter Estimation*, Society of Industrial and Applied Mathematics, Philadelphia, 2005.
[11] J. Beck, L. Katafygiotis, Updating and their uncertainties. I: *Bayesian statistical framework*, *Journal of Engineering Mechanics* (1998) 455–461.
[12] K.V. Yuen, *Bayesian Methods for Structural Dynamics and Civil Engineering*, John Wiley and Sons, Singapore, 2010.
[13] E. Zhang, P. Feissel, J. Antoni, A comprehensive Bayesian approach for model updating and quantification of modeling errors, *Probabilistic Engineering Mechanics* 26 (2011) 550–560.

[14] M. Williams, R. Landel, J. Ferry, The temperature dependence of relaxation mechanisms in amorphous polymers and other glass-forming liquids, *Journal of American Chemical Society* 77 (1955) 3701–3707.
[15] T. Pritz, Five-parameter fractional derivative model for polymeric damping materials, *Journal of Sound and Vibration* 265 (2003) 935–952.
[16] M. Sulmoni, T. Gmür, J. Cugnoni, M. Matter, Modal validation of sandwich shell finite elements based on a p-order shear deformation theory including zigzag terms, *International Journal for Numerical Methods in Engineering* 75 (2008) 1301–1319.
[17] J. Chazot, B. Nennig, A. Chettah, Harmonic response computation of viscoelastic multilayered structures using a ZPST shell element, *Computers and Structures* 89 (2011) 2522–2530.
[18] P. Avery, C. Farhat, G. Reese, Fast frequency sweep computations using a multi-point padé-based reconstruction method and an efficient iterative solver, *International Journal for Numerical Methods in Engineering* 69 (2007) 2848–2875.
[19] L.O. Chua, C.Y. Ng, Frequency domain analysis of nonlinear systems: *general theory*, *Electronic Circuits and Systems* 3 (1979) 165–185.
[20] R. Pintelon, J. Schoukens, *System Identification*: *A Frequency Domain Approach*, Second Edition, Wiley-IEEE Press, New Jersey, 2012.
[21] K. Worden, G.R. Tomlinson, *Nonlinearity in Structural Dynamics*: *Detection, Identification and Modelling*, Taylor and Francis, 2001.
[22] J.A. Rice, *Mathematical Statistics and Data Analysis*, Duxbury Press, Belmont, 1995.
[23] R.H. Myers, D.C. Montgomery, *Response Surface Methodology*: *Process and Product Optimization using Designed Experiments*, John Wiley and Sons, New Jersey, 2002.
[24] R. Ghanem, P.D. Spanos, Design and analysis of computer experiments, *Journal of Applied Mechanics* 57 (1990) 197–202.
[25] J. Sacks, W.J. Welch, T.J. Mitchell, H.P. Wynn, Design and analysis of computer experiments, *Statistical Science* 4 (1989) 409–435.
[26] S. Haykin, *Neural Networks*: *A Comprehensive Foundation*, Prentice Hall, Upper Saddle River, New Jersey, 1994.
[27] I.T. Nabney, *NETLAB Algorithms for Pattern Recognition*, Springer Verlag, London, 2003.
[28] F. Gamboa, E. Gassiat, Bayesian methods and maximum entropy for ill-posed inverse problems, *The Annals of Statistics* 25 (1997) 328–350.
[29] P. Henrici, *Applied and Computational Complex Analysis*, John Wiley and Sons, New York, 1974.
[30] B. Gustavsen, A. Semlyen, Rational approximation of frequency domain responses by vector fitting, *International Journal for Numerical Methods in Engineering* 14 (1999) 1052–1061.
[31] M.E. Tipping, C.M. Bishop, Mixtures of probabilistic principal component analysers, *Neural Computation* 11 (1999) 443–482.
[32] Y.M. Shi, H. Sol, H.X. Hua, Material parameter identification of sandwich beams by an inverse method, *Journal of Sound and Vibration* 290 (2006) 1234–1255.
[33] N. Metropolis, A.W. Rosenbluth, M.N. Teller, Equations of state calculations by fast computing machines, *Journal of Chemical Physics* 21 (1953) 1087–1091.
[34] W.R. Gilks, S. Richardson, D. Spiegelhalter, *Markov Chain Monte Carlo in Practice*, Chapman and Hall, London, 1995.
[35] F. Liang, W.H. Wong, Real-parameter evolutionary Monte Carlo with applications to Bayesian mixture models, *Journal of the American Statistical Association* 96 (2001) 653–666.
[36] B.T. Zhang, D.Y. Cho, System identification using evolutionary Markov Chain Monte Carlo, *Journal of Systems Architecture* 47 (2001) 587–599.
[37] B. Hu, K.W. Tsui, Distributed evolutionary Monte Carlo for Bayesian computing, *Computational Statistics and Data Analysis* 54 (2010) 688–697.
[38] C.J. Geyer, Markov Chain Monte Carlo maximum likelihood, computing science and statistics, *Proceeds of 23rd Symposium on the Interface*, Interface Foundation, Fairfax Station, pp. 156–163.
[39] M.P. Wand, M.C. Jones, *Kernel Smoothing*, Chapman and Hall/CRC, London, 1995.
[40] ISO/PAS Standard 16940, Glass in Building – Glazing and Airborne Sound Insulation – Measurement of the Mechanical Impedance of Laminated Glass, International Organization for Standardization, 2004.